

Protein functionalized nanostructured zirconia based electrochemical immunosensor for cardiac troponin I detection

Suveen Kumar, Saurabh Kumar, Shine Augustine, and Banshi D. Malhotra^{a)}

Nano-bioelectronics Laboratory, Department of Biotechnology, Delhi Technological University, Delhi 110 042, India

(Received 25 January 2017; accepted 8 March 2017)

We report results of the studies relating to the fabrication of nanostructured zirconia ($n\text{ZrO}_2$) based immunosensor for cardiac troponin I biomarker (acute myocardial infarction) detection. One step, low temperature hydrothermal process was used for the synthesis of $n\text{ZrO}_2$ (~ 5 nm). This $n\text{ZrO}_2$ was functionalized with 3-aminopropyl triethoxy silane (APTES) and thereafter it was electrophoretically deposited on to indium tin oxide (ITO) coated glass electrode. EDC/NHS surface chemistry was used for covalent immobilization of monoclonal anti-troponin-I (anti-cTnI) antibodies onto APTES/ $n\text{ZrO}_2$ /ITO electrode. The structural, morphological and functional characterization of the synthesized nanoparticles and the fabricated immunoelectrode were conducted via X-ray diffraction (XRD), transmission electron microscopy (TEM), Fourier transform infrared spectroscopy (FTIR), and electrochemical techniques. The results of electrochemical response studies of BSA/anti-cTnI/APTES/ $n\text{ZrO}_2$ /ITO immunoelectrode reveal that, this platform can be used for efficient detection of cardiac troponin I (cTnI) biomarker with a wide linear detection range (0.1–100 ng/mL) and sensitivity [$3.9 \mu\text{A mL}/(\text{ng cm}^2)$].

I. INTRODUCTION

Among the various cardiovascular diseases, acute myocardial infarction (AMI) is currently one of the leading cause of death worldwide.^{1,2} The main symptoms associated with AMI are chest pain, shortness of breath, nausea, heartburn etc. that occur due to the blocking of blood flow in the circulatory system.³ High level of cholesterol present in blood leads to the blockage of coronary artery resulting in damage of cardiac muscles.^{2,3} Troponin is an integral protein present in each myofibril and helps in contraction of the cardiac muscles.⁴ It is a complex of three regulatory proteins: troponin C, troponin T, and troponin I.⁴ Among these, cardiac troponin I (cTnI) is released in the bloodstream when cardiac muscle is damaged or dead.⁵ Therefore, cTnI is presently a gold standard for the confirmation of cardiac tissue injury and can be used as an early diagnosis of AMI.⁶ cTnI is a water soluble proteinaceous biomarker having molecular weight of 21 kDa and is secreted in blood serum.⁷ The cutoff concentration of cTnI protein in the blood serum is found to be in the range, 0.01–0.1 ng/mL and increases upto 100 ng/mL in a heart patient.⁵ The initial time of cTnI elevation in blood has been found to be 4–6 h and returns to normal level in 6–8 days.⁵ For the detection of cTnI many immunoassay techniques such as

radioactive immune assay (RIA), fluoro-immuno assay, immuno-electrophoresis, spectro-photometric methods, electrochemiluminescence assays, radioimmunoassay, enzyme linked immunosorbent assay (ELISA) etc. can be used.^{8–11} These methods are time-consuming, expensive, and require highly skilled personnel. In this context, biosensors offer a simple reliable and user friendly detection strategy with increased assay speed, high sensitivity, and require low sample volumes.^{12–15}

For the fabrication of efficient biosensors immobilization matrix plays an important role.¹⁶ Nanomaterials can provide suitable platforms for the immobilization of biomolecules on desired substrate. These substrates can be used for monitoring of an electrical signal resulting due to an electrochemical reaction at an electrode surface, usually as a result of an applied potential, current, or frequency. The unique optical, electrical, and molecular properties of these materials can be helpful in improving the biosensing parameters.^{16–18} In last two decades, nanostructured metal oxides (NMOs) are widely used as an immobilization matrix.^{16,19} These interesting nanomaterials exhibit interesting optical and electrical properties due to electron and phonon confinement, high surface reaction activity, modified surface work function, high surface-to-volume ratio, high catalytic efficiency, and strong adsorption ability.¹⁶ Several NMOs based on iron oxide (Fe_3O_4), zinc oxide (ZnO), titanium oxide (TiO_2), copper oxide (CuO), cerium oxide (CeO_2), magnesium oxide (MgO), aluminum oxide (Al_2O_3), nickel oxide (NiO), hafnium oxide (HfO_2), zirconium

Contributing Editor: Venkatesan Renugopalakrishnan

^{a)}Address all correspondence to this author.

e-mail: bansi.malhotra@gmail.com

DOI: 10.1557/jmr.2017.102

oxide (ZrO_2) etc. have been used for the development of various biosensors.^{14,20–22} Nanostructured zirconium oxide (nZrO_2) has emerged as an interesting material due to its excellent electrochemical properties, reduced leaching current, chemically inert, facile electron transfer rate, and excellent electrical, biocompatibility, and surface charge properties. Moreover, the presence of oxygen moieties in nZrO_2 allows efficient covalent bonding with silane compound and ITO surface.^{20,23}

We report for the first time the application of nanostructured zirconia (nZrO_2) as an immobilization matrix for the development of a simple and label-free electrochemical immunosensor for the detection of cardiac biomarker, cTnI. The fabricated immunosensor shows remarkable sensitivity [$3.9 \mu\text{A mL}/(\text{ng cm}^2)$] and wide linear detection range (0.1–100 ng/mL).

II. MATERIALS AND METHODS

A. Chemicals and biomolecules

Zirconium tetraethoxide [$\text{Zr}(\text{OC}_2\text{H}_5)_4$], 3-aminopropyl triethoxy silane (APTES), bovine serum albumin (BSA) and 1-(3-(dimethylamino)-propyl)-3-ethylcarbodiimide hydrochloride (EDC) [$\text{C}_8\text{H}_{17}\text{N}_3$] were procured from Sigma-Aldrich (St. Louis, Missouri). Acetonitrile anhydrous (CH_3CN), cetyltrimethylammonium bromide (CTAB) [$\text{C}_{19}\text{H}_{42}\text{BrN}$], sodium hydroxide (NaOH), sodium monophosphate [NaH_2PO_4], sodium diphosphate dihydrate [$\text{Na}_2\text{HPO}_4 \cdot 2\text{H}_2\text{O}$], *N*-hydroxysuccinimide (NHS) [$\text{C}_4\text{H}_5\text{NO}_3$], sodium chloride [NaCl], potassium ferricyanide [$\text{K}_3[\text{Fe}(\text{CN})_6]$], and potassium ferrocyanide [$\text{K}_4[\text{Fe}(\text{CN})_6] \cdot 3\text{H}_2\text{O}$] were purchased from Merck India Pvt. Limited (Mumbai, India). All chemicals were of analytical grade and were used without any further purification. Cardiac troponin-I (cTnI) and mouse monoclonal anti-cardiac troponin I (anti-cTnI) were procured from GeneTex (Irvine, California). Phosphate buffer saline (PBS) solutions of different pH were prepared using $\text{Na}_2\text{HPO}_4 \cdot 2\text{H}_2\text{O}$ and NaH_2PO_4 in deionized water of resistivity (18 M Ω cm). Dilutions of biomolecules were prepared in PBS (pH 7.0) buffer and stored at 4 °C till further use.

B. Synthesis of ZrO_2 nanoparticles (nZrO_2)

One step low temperature hydrothermal process was used to synthesize ZrO_2 nanoparticles. For this purpose, a mixed solution of 0.1 M zirconium ethoxide, 0.4 M NaOH, and 0.1 M CTAB was prepared and stirred continuously for 2 h. Further, the solution was kept in a water bath for 1 h at 100 °C and then it was immediately cooled under running tap water. Subsequently, the prepared solution was transferred to a teflon coated stainless steel autoclave vessel and kept in hydrothermal oven at 170 °C for 15 h. After cooling, the resulting

solution was washed 3–4 times with deionized water followed by ethanol. Thus obtained pellet was dried in an oven at 80 °C and it was further kept in furnace at 400 °C for 3 h for removing impurities. The whitish product was crushed into fine powder and stored in dark, cool, and dry place for further use.

C. Surface modification of nZrO_2

3-Aminopropyltriethoxy silane (APTES) was used to modify the surface of nZrO_2 with amine ($-\text{NH}_2$) terminal. 100 mg of nZrO_2 was added into 20 mL of isopropanol and sonicated for 15 min to obtain dispersed homogenous solution. Further, 200 μL of APTES and 5 mL of deionized water were added and kept for constant stirring at 300 rpm for 48 h at 50 °C. The obtained pellets were washed with deionized water. The Whatman filter paper was used to remove any unbound APTES molecules and further stored in cool and dry place.

D. Electrophoretic deposition of APTES/ nZrO_2 onto ITO electrodes

Indium tin oxide (ITO) coated glass electrode was used to fabricate thin films of functionalized nZrO_2 (APTES/ nZrO_2). The hydrolyzed ITO electrode was used for electrophoretic deposition (EPD) of APTES/ nZrO_2 . For EPD, colloidal suspensions (1 mg/mL) of APTES/ nZrO_2 in acetonitrile was prepared and further a potential of 15 V for 3 min was applied in a two electrode system where ITO was used as cathode and platinum wire as anode kept at a distance of 1 cm. The uniform thin films of APTES/ nZrO_2 were obtained and were further used for covalent immobilization of anti-cTnI.

E. Fabrication of BSA/anti-cTnI/APTES/ nZrO_2 /ITO electrodes

Monoclonal anti-cTnI (50 $\mu\text{g}/\text{mL}$) antibodies were covalently immobilized onto APTES/ nZrO_2 /ITO electrodes. Prior to this, the carboxyl group of Fc region of anti-cTnI was activated by using the EDC and NHS chemistry. A mixed solution of anti-cTnI:EDC:NHS (2:1:1) (30 μL) was prepared and kept at 25 °C for 30 min. Thereafter the mixed solution was uniformly spread onto APTES/ nZrO_2 /ITO electrode. The electrode was incubated at room temperature under humid conditions for 3 h. After completion of the incubation period, the electrode was washed with PBS. Further 20 μL of BSA (0.1 mg/mL) was used for blocking of the non-specific binding sites of the immunoelectrode (anti-cTnI/APTES/ nZrO_2 /ITO). The prepared BSA/anti-cTnI/APTES/ nZrO_2 /ITO immunoelectrode was further washed with PBS and stored at 4 °C till further use.

F. Characterization

Crystallinity and phase determination of synthesized $n\text{ZrO}_2$ were determined by X-ray diffraction (XRD; $\text{Cu K}\alpha$ radiations, Bruker D-8 Advance, Bruker, Karlsruhe, Germany). Structural and surface morphology of electrodes, before and after immobilization of the antibodies was investigated by using scanning electron microscopy (SEM; Hitachi-3700N, Hitachi Corp., Tokyo, Japan) and transmission electron microscopy (TEM; JEM-2100F-TEM system, JEOL Ltd., Tokyo, Japan). Electrochemical characterization and response studies were carried out using cyclic voltammetry (CV)

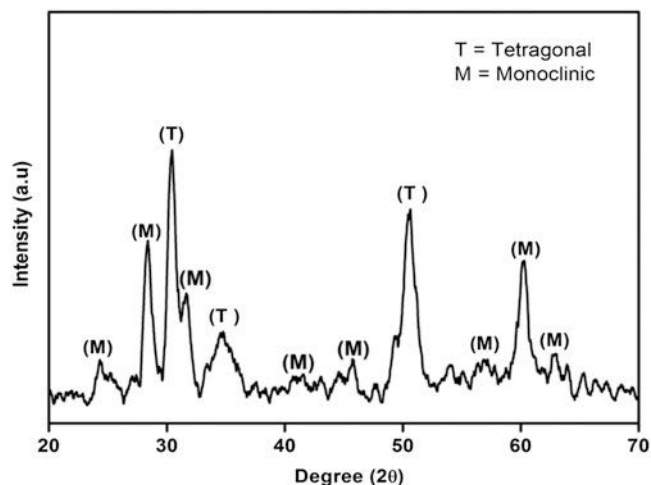


FIG. 1. XRD pattern of $n\text{ZrO}_2$.

technique on an Autolab Potentiostat (Metrohm Autolab B.V., Utrecht, The Netherlands) with a conventional three-electrode system having ITO coated glass electrode (working electrode), platinum (counter electrode), and silver-silver chloride (Ag/AgCl) (reference electrode) in phosphate buffer saline (50 mM, pH 7.0) containing 5 mM $[\text{Fe}(\text{CN})_6]^{3-/4-}$.

III. RESULTS AND DISCUSSION

A. X-ray diffraction (XRD) studies

The phase determination of the synthesized material was examined through XRD pattern with 2θ angle from 20° to 70° (Fig. 1). The peaks present at 2θ angles are 30.17 , 50.17 , and 34.63 corresponding to the planes (101), (200), and (002), respectively (JCPDS No. 81-1544), indicating the tetragonal phase of zirconia nanoparticles. However, the peaks seen at 2θ angles are 24.44 , 28.17 , 31.46 , 60.0 , 41.37 , 45.5 , 57.1 , and 62.8 corresponded to the planes (110), (111), (111), (302), (121), (211), (311), and (312), respectively (JCPDS No. 78-1807), indicating the monoclinic phase of zirconia nanoparticles. These results revealed the formation of the mixed phase (i.e., tetragonal and monoclinic) zirconia. Further, the average crystalline size of the synthesized material was calculated to be 5 nm through Scherer equation i.e., $D = 0.9\lambda/\beta \cos \theta$ where D is particle size of the materials, λ ($=1.5460 \text{ \AA}$) is the wave length of target $\text{Cu K}\alpha$, β is the full width half maximum of diffraction peak, and θ is the Bragg's angle of diffraction.

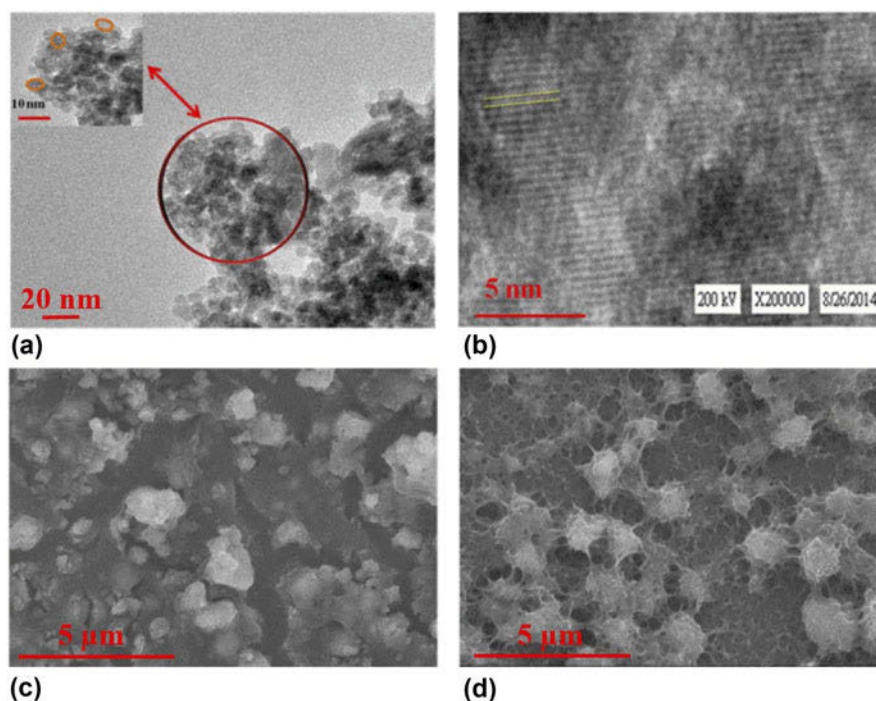


FIG. 2. (a and b) TEM images of $n\text{ZrO}_2$, (c and d images) SEM images showing APTES/ $n\text{ZrO}_2$ /ITO and anti-cTnI/APTES/ $n\text{ZrO}_2$ /ITO electrodes.

B. Morphological studies

TEM and HR-TEM studies were carried out to examine the size and shape of synthesized $n\text{ZrO}_2$. Figure 2(a) reveals the spherical structure of $n\text{ZrO}_2$ with an average particle size of ~ 5 nm. The magnified image (inset) of $n\text{ZrO}_2$ exhibits spherical shapes arranged in random orientation, which are marked by the orange line. Figure 2(b) shows lattice fringes of $n\text{ZrO}_2$ revealing crystalline nature of $n\text{ZrO}_2$. The distance between two lattice spacing was obtained to be 0.214 nm. The surface morphology of various modified electrodes was investigated using SEM. Figure 2(c) shows SEM of APTES/ $n\text{ZrO}_2$ /ITO electrode, wherein APTES/ $n\text{ZrO}_2$ appears to be in clustered form. However, morphology of the anti-cTnI/APTES/ $n\text{ZrO}_2$ /ITO [Fig. 2(d)] appears as globular network like structure with several bunches that are connected with each other in network like fashion, indicating successful attachment of anti-cTnI.

C. Electrochemical studies

Electrochemical studies of the fabricated electrodes were carried out in PBS containing 5 mM $[\text{Fe}(\text{CN})_6]^{3-/4-}$. Cyclic voltammetry (CV) was used to investigate the electrochemical response of the fabricated electrode. The effect of pH on the electrochemical response of the fabricated BSA/anti-cTnI/APTES/ $n\text{ZrO}_2$ /ITO electrode was studied through CV at scan rate of 50 mV/s as shown in Fig. 3. The maximum peak current was obtained at pH 7.0 (Inset, Fig. 3). This could perhaps be due to the fact that a biological molecule retains its maximum activity at neutral pH (pH 7.0). However, the acidic or basic medium biomolecules perhaps get denatured. Therefore all electrochemical studies were conducted in PBS with pH 7.0.

Figure 4 shows results of CV studies conducted on ITO, $n\text{ZrO}_2$ /ITO, APTES/ $n\text{ZrO}_2$ /ITO, anti-cTnI/APTES/ $n\text{ZrO}_2$ /ITO, and BSA/anti-cTnI/APTES/ $n\text{ZrO}_2$ /ITO

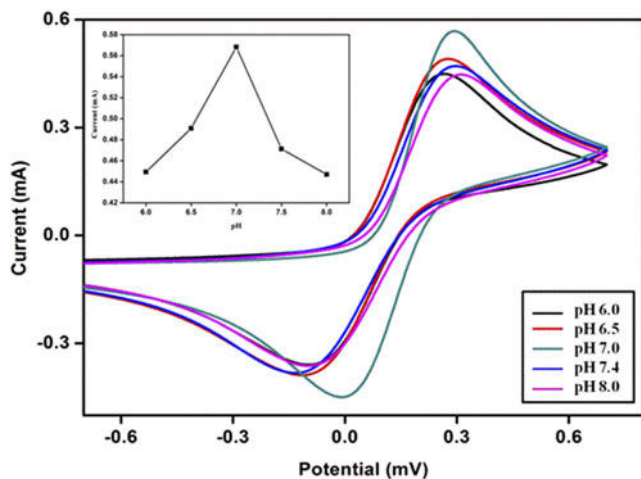


FIG. 3. Current response of the BSA/anti-cTnI/APTES/ $n\text{ZrO}_2$ /ITO immunoelectrode as a function of pH.

electrode, respectively. It can be seen that the peak current of $n\text{ZrO}_2$ /ITO electrode (0.59 mA) is higher with respect to that of ITO electrode (0.53 mA). This increase in peak current is due to the cationic nature of $n\text{ZrO}_2$. After deposition of APTES functionalized $n\text{ZrO}_2$ onto ITO electrode, the peak current (0.63 mA) increased in comparison with that of $n\text{ZrO}_2$ /ITO electrode (0.59 mA). This can perhaps be attributed to increased electron transfer between solution and APTES/ $n\text{ZrO}_2$ /ITO electrode interface. However, after immobilization of anti-cTnI onto APTES/ $n\text{ZrO}_2$ /ITO electrode, the peak current decreased (0.59 mA) due to insulating behavior of the antibodies that act as a barrier toward the transportation of electrons from the bulk solution to the electrode surface.¹⁴ Further, after BSA immobilization onto the anti-cTnI/APTES/ $n\text{ZrO}_2$ /ITO immunoelectrode peak current decreased (0.57 mA). This is due to blocking of the nonspecific active sites of immunoelectrode.²³

The electrochemical response of the APTES/ $n\text{ZrO}_2$ /ITO and BSA/anti-cTnI/APTES/ $n\text{ZrO}_2$ /ITO electrode obtained as a function of scan rate (50–150 mV/s) is shown in Fig. 5. It was observed that the cathodic and anodic peak current increased linearly with square root of scan rate (Inset i, Figs. 5 and 6) indicating the electrochemical reaction as a diffusion controlled process. The slopes and intercepts are given by the Eqs. (1)–(4):

$$I_{pa(\text{APTES}/n\text{ZrO}_2/\text{ITO})} = [0.068 \text{ mA}(\text{s}/\text{mV}) \times (\text{scan rate}[\text{mV}/\text{s}])^{1/2}] + 0.149 \text{ mA}$$

$$R^2 = 0.999, \text{ SD} = 6.25 \times 10^{-4} \quad (1)$$

$$I_{pc(\text{APTES}/n\text{ZrO}_2/\text{ITO})} = -[0.048 \text{ mA}(\text{s}/\text{mV}) \times (\text{scan rate}[\text{mV}/\text{s}])^{1/2}] - 0.201 \text{ mA}$$

$$R^2 = 0.998, \text{ SD} = 6.72 \times 10^{-4} \quad (2)$$

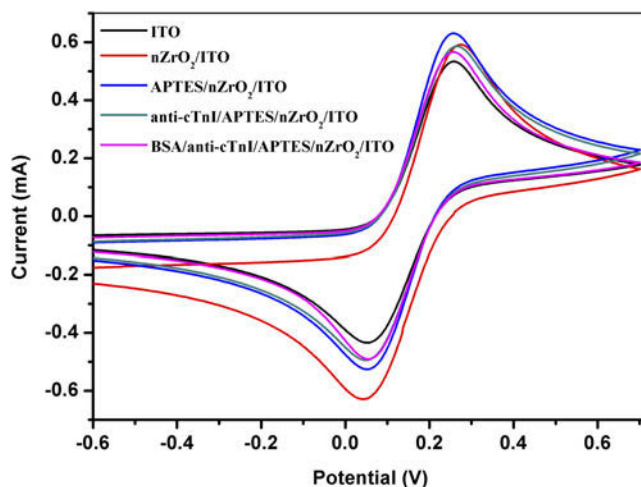


FIG. 4. Cyclic voltammogram (CV) of ITO, $n\text{ZrO}_2$ /ITO, APTES/ $n\text{ZrO}_2$ /ITO, anti-cTnI/APTES/ $n\text{ZrO}_2$ /ITO and BSA/anti-cTnI/APTES/ $n\text{ZrO}_2$ /ITO electrodes.

$$I_{pa}(\text{BSA/anti-cTnI/APTES/nZrO}_2/\text{ITO}) = [0.057 \text{ mA(s/mV)} \\ \times (\text{scan rate}[\text{mV/s}]^{1/2}) + 0.163 \text{ mA} \\ R^2 = 0.999, \text{ SD} = 5.05 \times 10^{-4} \quad (3)$$

$$I_{pc}(\text{BSA/anti-cTnI/APTES/nZrO}_2/\text{ITO}) = -[0.043 \text{ mA(s/mV)} \\ \times (\text{scan rate}[\text{mV/s}]^{1/2}) - 0.192 \text{ mA} \\ R^2 = 0.998, \text{ SD} = 5.90 \times 10^{-4} \quad (4)$$

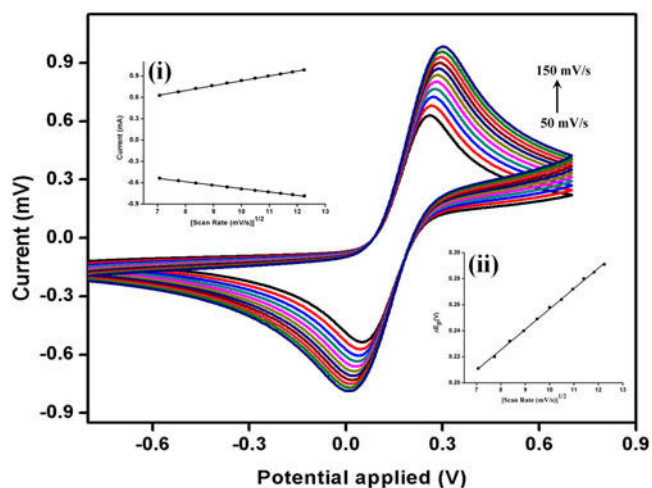


FIG. 5. Cyclic voltammetry (CV) of APTES/nZrO₂/ITO electrode as a function of scan rate (50–150 mV/s). Magnitude of oxidation and reduction current response as a function of square root of scan rate (mV/s) (inset i), and difference of cathodic and anodic peak potential (ΔE_p) as a function of square root of scan rate (inset ii).

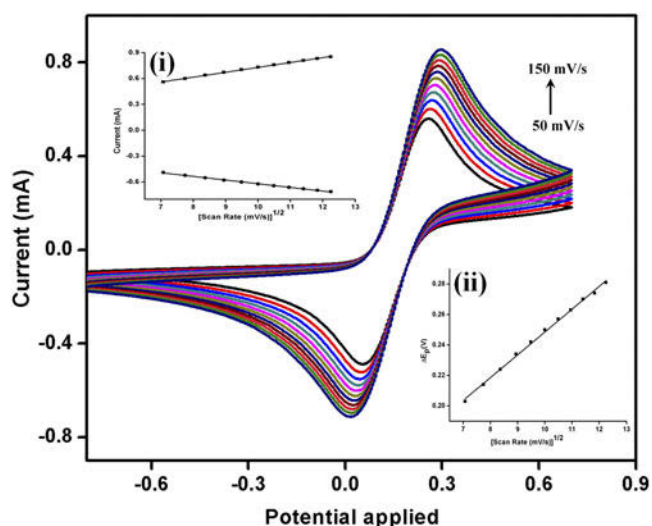


FIG. 6. Cyclic voltammetry (CV) of BSA/anti-cTnI/APTES/nZrO₂/ITO immunoelectrode as a function of scan rate (50–150 mV/s). Magnitude of oxidation and reduction current response as a function of square root of scan rate (mV/s) (inset i), and difference of cathodic and anodic peak potential (ΔE_p) as a function of square root of scan rate (inset ii).

The difference of cathodic (E_{pc}) and anodic (E_{pa}) peak potential ($\Delta E = E_{pc} - E_{pa}$) of both APTES/nZrO₂/ITO and BSA/anti-cTnI/APTES/nZrO₂/ITO electrodes shows the linear relationship with square root of scan rate (50–150 mV/s) and follows Eqs. (5) and (6) indicating facile electron transfer from medium to electrode surface (inset ii, Figs. 5 and 6).

$$\Delta E_p(\text{V})_{\text{APTES/nZrO}_2/\text{ITO}} = [0.0156 \text{ V(s/mV)} \\ \times (\text{scan rate}[\text{mV/s}]^{1/2}) + 0.099 \text{ V} , \\ R^2 = 0.999, \text{ SD} = 1.69 \times 10^{-4} \quad (5)$$

$$\Delta E_p(\text{V})_{\text{BSA/anti-cTnI/APTES/nZrO}_2/\text{ITO}} = [0.0149 \text{ V(s/mV)} \\ \times (\text{scan rate}[\text{mV/s}]^{1/2}) + 0.098 \text{ V} , \\ R^2 = 0.997, \text{ SD} = 2.42 \times 10^{-4} \quad (6)$$

D. Electrochemical response studies

The electrochemical response of BSA/cTnI/APTES/nZrO₂/ITO immunoelectrode was measured as a function of troponin I in the concentration range (0.1–100 ng/mL) in PBS containing $[\text{Fe}(\text{CN})_6]^{3-/4-}$ [5 mM] at a scan rate of 50 mV/s at a potential range –0.8 to 0.8 V using CV technique. It was observed that the anodic peak current increased linearly with increasing cTnI concentration from 0.1 ng/mL to 100 ng/mL (Fig. 7). Increase in anodic peak current with respect to cTnI concentration may be due to the formation of electron transfer accelerating layer by the interaction between the troponin I and anti-cTnI on the surface of

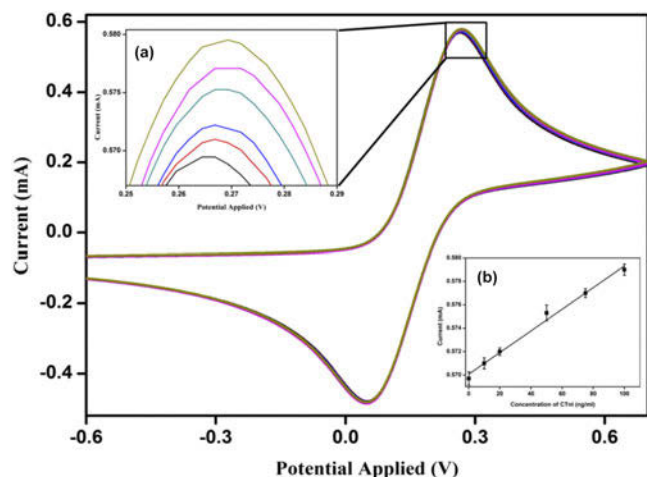


FIG. 7. Electrochemical response of BSA/anti-cTnI/APTES/nZrO₂/ITO immunoelectrode as a function of cTnI concentration (0.1–100 ng/mL). The magnified view of oxidation peak current (inset a), calibration curve between magnitude of peak current and concentration of cTnI.

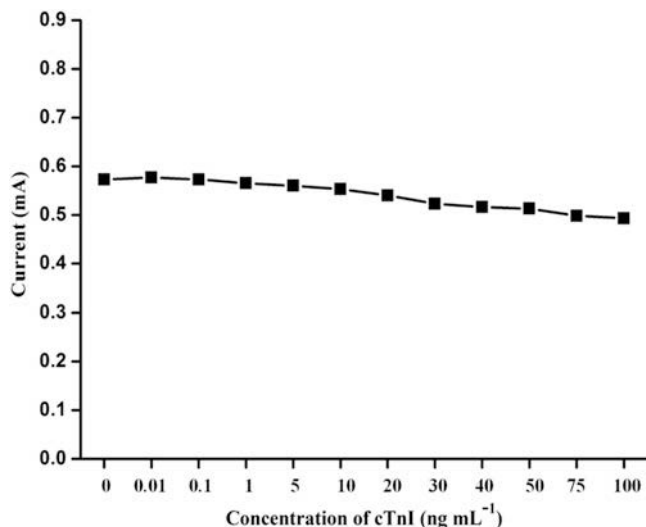


FIG. 8. Control experiment (through electrochemical response study) of APTES/nZrO₂/ITO electrode as a function of cTnI concentration (0–100 ng/mL).

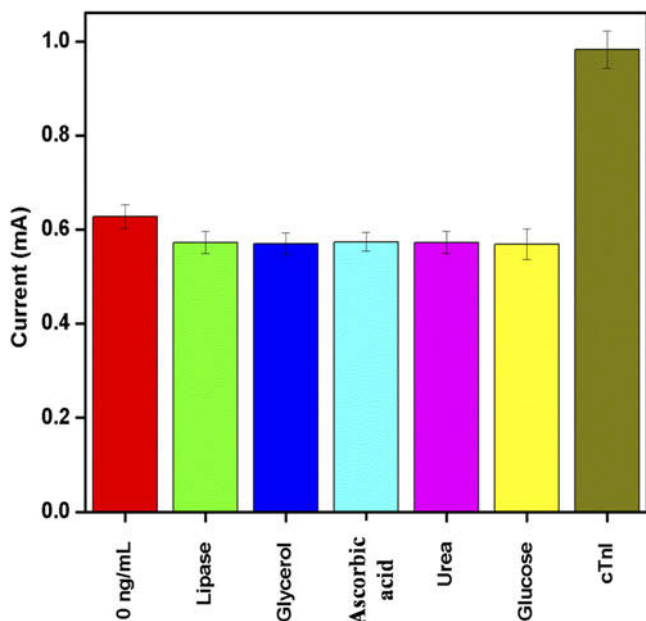


FIG. 9. Interferent studies of BSA/anti-cTnI/APTES/nZrO₂/ITO immunoelectrode.

BSA/cTnI/APTES/nZrO₂/ITO immunoelectrode. Moreover, troponin I is a polar protein molecule (isoelectric point ~9.9), having excess positively charged residues. Therefore, immunocomplex (positively charged) attracts the negatively charged redox probe [Fe(CN)₆]^{3-/4-} facilitating the redox reaction at the electrode surface leading to the increase in current on addition of troponin I (Inset i, Fig. 6). A linear relationship (0.1–100 ng/mL) between magnitude of current and cTnI concentration was observed with sensitivity 3.9 μA mL/(ng cm²) [Eq. (7)].

$$I_p = [(0.963 \mu\text{A mL/ng}) \times (\text{conc. of cTnI (ng/mL)})] + 0.569 \text{ mA} \quad , \quad R^2 = 0.98 \quad (7)$$

E. Control and interferences studies

A control experiment was performed using APTES/nZrO₂/ITO electrode as a function of different concentration of troponin I (Fig. 8). It was found that no significant changes occurred on addition of different concentration of troponin I. This indicated that APTES/nZrO₂/ITO electrode did not interact with antigen molecules.

We performed the interferent studies conducted on the BSA/cTnI/APTES/nZrO₂/ITO immunoelectrode using various potential interferents present in serum such as lipase, glucose, glycerol, urea, and ascorbic acid. Figure 9 shows results of the interferent studies obtained with different biomolecules and it can be seen that magnitude of anodic peak current increased after interaction with troponin I. However negligible change in current was observed upon addition of other interferent such as lipase, glucose, glycerol, urea, and ascorbic acid respectively indicating that the fabricated immunoelectrodes showed high selectivity toward troponin I biomolecules. The sensing characteristics of the proposed immunosensors have been summarized in Table I along with those reported in literature.

TABLE I. Comparative analysis of sensing characteristics of the fabricated biosensors with other reported literature for cTnI detection.

S. no.	Bioelectrode	Techniques	Label	Detection limit (ng/mL)	Linearity (ng/mL)	Sensitivity [μA mL/(ng cm)]	Reference
1	Silicon nanowire	FET nanodevice	No	0.092	0.092–46	...	T. Kong et al.
2	LC/AuNP/GC	Square wave voltammetry	No	0.076	0.1–0.9	...	Eduardo zapp et al.
3	MCM-MCPE	Anodic stripping voltammetry	Yes	0.5	0.8–5.0	...	Guo, H. et al.
4	GNP coated ITO	Electrochemical detection (open circuit potential)	Yes	...	1–100	...	A.J. Saleh Ahammad et al.
5	BSA/anti-cTnI/APTES/nZrO ₂ /ITO	Cyclic voltammetry	No	0.1	0.1–100	3.9	Present work

IV. CONCLUSION

We have fabricated a simple, efficient, label free nanostructured zirconia based immunosensor for acute myocardial infarction (AMI) detection. The nanostructured zirconia ($n\text{ZrO}_2$) has been synthesized via one step, low temperature hydrothermal process and further functionalized with APTES. Electrophoretic deposition (EPD) technique has been used for formation of the thin film of APTES/ $n\text{ZrO}_2$ onto ITO coated glass substrate. Further anti-cTnI has been immobilized onto the APTES/ $n\text{ZrO}_2$ /ITO electrode surface and BSA for blocking the nonspecific active sites. The fabricated BSA/cTnI/APTES/ $n\text{ZrO}_2$ /ITO immunoelectrode shows wide linear detection range (0.1–100 ng/mL) with high sensitivity [$3.9 \mu\text{A mL}/(\text{ng cm}^2)$]. Efforts should be made to investigate response of this immunosensors with the real sample cardiovascular patients.

ACKNOWLEDGMENTS

We thank Prof. Yogesh Singh, Vice-Chancellor, Delhi Technological University, Delhi (India) for providing the research facilities. Suveen Kumar and Saurabh Kumar are thankful to DTU for the award of financial assistance. Shine Augustine is thankful to UGC-MANF [2015-16/MANF-2015-17-DEL-55426] for financial assistance. We are also thankful to Mr. Sandeep Mishra (Central Instrument Facility, DTU) for XRD and SEM techniques.

REFERENCES

1. K. Thygesen, J.S. Alpert, A.S. Jaffe, M.L. Simoons, B.R. Chaitman, and H.D. White: Third universal definition of myocardial infarction. *Circulation* **126**, 2020 (2012).
2. F. Lanas, A. Avezum, L.E. Bautista, R. Diaz, M. Luna, S. Islam, and S. Yusuf: Risk factors for acute myocardial infarction in Latin America the INTERHEART Latin American study. *Circulation* **115**, 1067 (2007).
3. J.C. Barefoot and M. Schroll: Symptoms of depression, acute myocardial infarction, and total mortality in a community sample. *Circulation* **93**, 1976 (1996).
4. J. Sarko and C.V. Pollack: Cardiac troponins. *J. Emerg. Med.* **23**, 57 (2002).
5. M. Pedrero, S. Campuzano, and J.M. Pingarrón: Electrochemical biosensors for the determination of cardiovascular markers: A review. *Electroanalysis* **26**, 1132 (2014).
6. M.C. Fishbein, T. Wang, M. Matijasevic, L. Hong, and F.S. Apple: Myocardial tissue troponins T and I: An immunohistochemical study in experimental models of myocardial ischemia. *Cardiovasc. Pathol.* **12**, 65 (2003).
7. A.H. Wu, Y-J. Feng, R. Moore, F.S. Apple, P.H. McPherson, K.F. Buechler, and G. Bodor: Characterization of cardiac troponin subunit release into serum after acute myocardial infarction and comparison of assays for troponin T and I. *Clin. Chem.* **44**, 1198 (1998).
8. J. Wang, A. Ibáñez, M.P. Chatrathi, and A. Escarpa: Electrochemical enzyme immunoassays on microchip platforms. *Anal. Chem.* **73**, 5323 (2001).
9. M.A. Hayes, M.M. Petkus, A.A. Garcia, T. Taylor, and P. Mahanti: Demonstration of sandwich and competitive modulated supraparticle fluoroimmunoassay applied to cardiac protein biomarker myoglobin. *Analyst* **134**, 533 (2009).
10. T. Shiomi, M. Matsui, F. Mizukami, and K. Sakaguchi: A method for the molecular imprinting of hemoglobin on silica surfaces using silanes. *Biomaterials* **26**, 5564 (2005).
11. W. Shen, D. Tian, H. Cui, D. Yang, and Z. Bian: Nanoparticle-based electrochemiluminescence immunosensor with enhanced sensitivity for cardiac troponin I using *N*-(aminobutyl)-*N*-(ethylisoluminol)-functionalized gold nanoparticles as labels. *Biosens. Bioelectron.* **27**, 18 (2011).
12. A. Bogomolova, E. Komarova, K. Reber, T. Gerasimov, O. Yavuz, S. Bhatt, and M. Aldissi: Challenges of electrochemical impedance spectroscopy in protein biosensing. *Anal. Chem.* **81**, 3944 (2009).
13. S. Kumar, J.G. Sharma, S. Maji, and B.D. Malhotra: A biocompatible serine functionalized nanostructured zirconia based biosensing platform for non-invasive oral cancer detection. *RSC Adv.* **6**, 77037 (2016).
14. S. Kumar, S. Kumar, S. Tiwari, S. Augustine, S. Srivastava, B.K. Yadav, and B.D. Malhotra: Highly sensitive protein functionalized nanostructured hafnium oxide based biosensing platform for non-invasive oral cancer detection. *Sens. Actuators, B* **235**, 1 (2016).
15. A. Chaubey and B. Malhotra: Mediated biosensors. *Biosens. Bioelectron.* **17**, 441 (2002).
16. P.R. Solanki, A. Kaushik, V.V. Agrawal, and B.D. Malhotra: Nanostructured metal oxide-based biosensors. *NPG Asia Mater.* **3**, 17 (2011).
17. S. Kumar, J.G. Sharma, S. Maji, and B.D. Malhotra: Nanostructured zirconia decorated reduced graphene oxide based efficient biosensing platform for non-invasive oral cancer detection. *Biosens. Bioelectron.* **78**, 497 (2016).
18. S. Kumar, S. Kumar, S. Srivastava, B.K. Yadav, S.H. Lee, J.G. Sharma, D.C. Doval, and B.D. Malhotra: Reduced graphene oxide modified smart conducting paper for cancer biosensor. *Biosens. Bioelectron.* **73**, 114 (2015).
19. K.K. Tadi, T.N. Narayanan, S. Arepalli, K. Banerjee, S. Viswanathan, D. Liepmann, P.M. Ajayan, and V. Rengopalakrishnan: Engineered 2D nanomaterials-protein interfaces for efficient sensors. *J. Mater. Res.* **30**, 3565 (2015).
20. M. Das, C. Dhand, G. Sumana, A. Srivastava, R. Nagarajan, L. Nain, M. Iwamoto, T. Manaka, and B. Malhotra: Electrophoretic fabrication of chitosan-zirconium-oxide nanobiocomposite platform for nucleic acid detection. *Biomacromolecules* **12**, 540 (2011).
21. A. Kaushik, R. Khan, P.R. Solanki, P. Pandey, J. Alam, S. Ahmad, and B. Malhotra: Iron oxide nanoparticles-chitosan composite based glucose biosensor. *Biosens. Bioelectron.* **24**, 676 (2008).
22. A.A. Ansari, G. Sumana, M. Pandey, and B. Malhotra: Sol-gel-derived titanium oxide-cerium oxide biocompatible nanocomposite film for urea sensor. *J. Mater. Res.* **24**, 1667 (2009).
23. S. Kumar, S. Kumar, S. Tiwari, S. Srivastava, M. Srivastava, B.K. Yadav, S. Kumar, T.T. Tran, A.K. Dewan, and A. Mulchandani, J.G. Sharma, S. Maji, and B.D. Malhotra: Biofunctionalized nanostructured zirconia for biomedical application: A smart approach for oral cancer detection. *Adv. Sci.* **2**, 1500048 (2015).